Nano Energy 86 (2021) 106035

Contents lists available at ScienceDirect

Nano Energy

journal homepage: http://www.elsevier.com/locate/nanoen

Full paper

Machine learning-enabled textile-based graphene gas sensing with energy harvesting-assisted IoT application

Jianxiong Zhu [a,b,d,1], Minkyu Cho [b,1], Yutao Li [c], Tianyiyi He [d], Junseong Ahn [b], Jaeho Park [b], Tian-Ling Ren [c], Chengkuo Lee [d,*], Inkyu Park [b,*]

[a] School of Mechanical Engineering, Southeast University, Nanjing 211189, China
[b] Mechanical Engineering and KI for NanoCentry, Korea Advanced Institute of Science and Technology (KAIST), Daejeon 34141, Republic of Korea
[c] Institute of Microelectronics, Tsinghua University, Beijing 100084, China
[d] Department of Electrical and Computer Engineering, National University of Singapore, Singapore 117576, Singapore

ARTICLE INFO

Keywords:
Machine learning
Internet of things
Graphene sensor
Extremely deformation
Inkjet-printing

ABSTRACT

Flexible gas sensing is attracting more attention with the development of machine learning and Internet of Things (IoT). Herein, we report flexible and foldable high-performance hydrogen (H_2) sensor on all textiles substrate-fabricated by inkjet–printing of reduced graphene oxide (rGO) and its application to wearable environmental sensing. The inkjet-printing process provides the advantages of the compatibility with various substrates, the capability of non-contact patterning and cost-effectiveness. The sensing mechanism is based on the catalytic effect of palladium (Pd) nanoparticles (NPs) on the wide bandgap rGO, which allows facile adsorption and desorption of the nonpolar H_2 molecules. The graphene textile gas sensor (GT-GS) demonstrates about six times higher sensing response than the graphene polyimide membrane gas sensor due to the large surface area of the textile substrate. An analysis of the temperature influence on the GT-GS shows better H_2 gas response at room temperature than at high temperature (e.g., 120 °C). In addition, with the machine learning-enabled technology and triboelectric-textile to power IoT (temperature and humidity for gas calibration), H_2 is well identified for wearable applications with a robust mechanical performance (e.g., flexibility and foldability).

1. Introduction

Hydrogen (H_2) is used widely in the area including the metal production, semiconductor manufacturing, hydrogen-based energy generation systems, etc. Unfortunately, high concentration H_2 gas can cause serious explosion in case of leakage due to its high flammability. However, it is impossible for ordinary human senses to detect H_2 because of its colorless and odorless nature, and therefore developing a high response H_2 sensor is essential for the improved safety of the hydrogen industry [1–3]. Over the past several decades, researchers have developed various kinds of H_2 sensing principles based on electrochemical sensing, chemoresistive sensing, catalytic combustion sensing, optical sensing, etc [4–9]. Chemoresistive sensor is the most traditional one, which is measuring the change of electrical resistance in response to the nearby chemical environment. Among typical chemoresistive materials including metal oxides, conductive polymers, carbon nanotubes, graphene, etc., graphene has mechanically flexible 2D structures, large surface area, and high electron mobility [10–15]. In particular, the graphene/palladium (Pd) composite has been demonstrated to be a sensitive functional material due to its strong chemical reaction to hydrogen atoms, which makes it a promising material for H_2 gas sensors [16–22]. Additionally, the 3D graphene composite microstructure provides much larger surface area for the gas sensing than a 1D graphene quantum point or a 2D graphene film, which can dramatically improve the gas sensing performance [16,17,19,20].

Researchers have carried out many studies on the graphene/Pd composite for gas sensing applications [8,23–43]. Wolfbeis, et al. first reported a graphene/Pd composite for an H_2 sensor in 2011 with a 4% response (graphene) and 35% response (graphene/Pd) for 1% H_2, respectively [34]. However, the seven or ten layers graphene by hummer method is complicated and expensive for the production. Meanwhile, many other research groups have tried to increase the response by implementing larger surface area in the microstructure with cheap price [32,33]. For example, Lupan et al. introduced an ultra-light 3D

* Corresponding authors.
E-mail addresses: elelc@nus.edu.sg (C. Lee), inkyu@kaist.ac.kr (I. Park).
[1] Jianxiong Zhu, and Minkyu Cho contributed equally to this work.

https://doi.org/10.1016/j.nanoen.2021.106035
Received 12 February 2021; Received in revised form 24 March 2021; Accepted 28 March 2021
Available online 20 April 2021

micro-tube network of aerographite for H_2 detection [32]. The response of H_2 sensors has been improved over that of a flat graphite film due to the large surface area of the 3D micro-tube network. Raston, et al. introduced an rGO/Pd sheet composite for H_2 sensing; however, their device obtained about 8% response with a 1% H_2 exposure, and their complicated MEMS-based manufacturing process constrained their commercial applications [42]. Printing techniques, such as inkjet-printing, are competitive alternatives to conventional microfabrication processes for the gas sensor fabrication [44–57]. Compared to other printing techniques (e.g., screen printing and microcontact printing), inkjet-printing has attracted more attention due to its significant advantages such as compatibility with various substrates and cost-effectiveness.

As a fast technology development of the fifth-generation cellular network technology (5 G), everything is connecting in a much easier way by the Internet of Things (IoT), especially the power source from triboelectric effect [1–4,58–67]. In addition, the artificial intelligence (AI) enabled data analytics at the cloud server realize new artificial intelligence of things (AIoT) technology, where low-cost and flexible sensors collect sensory information and send to the cloud wirelessly. Machine learning approaches help the remote data analysis to be exercised in cloud. Leveraging the future 5 G and AIoT technologies, the H_2 sensor is strongly demanded because the personal healthcare applications look for real-time monitoring. Thus, to visualize the big data from sensor, principal component analysis (PCA) is a useful tool for the scientific study of algorithms and statistical models enable hydrogen detection for extreme deformed environment applications. This paper introduces a foldable reduced graphene oxide (rGO) based H_2 sensor on a textile substrate using inkjet printing and its wearable device applications. The inkjet-printing enables facile and flexible pattern generation on a textile substrate. Also, due to the porous and rough surface of the textile substrate, the rGO gas sensor on a textile substrate exhibits about six time's higher sensing response than the rGO sensor on a PI film. The textile substrate demonstrated better mechanical robustness compared to the paper microfiber based substrate. Furthermore, with the machine learning-enabled principal component analysis (PCA)

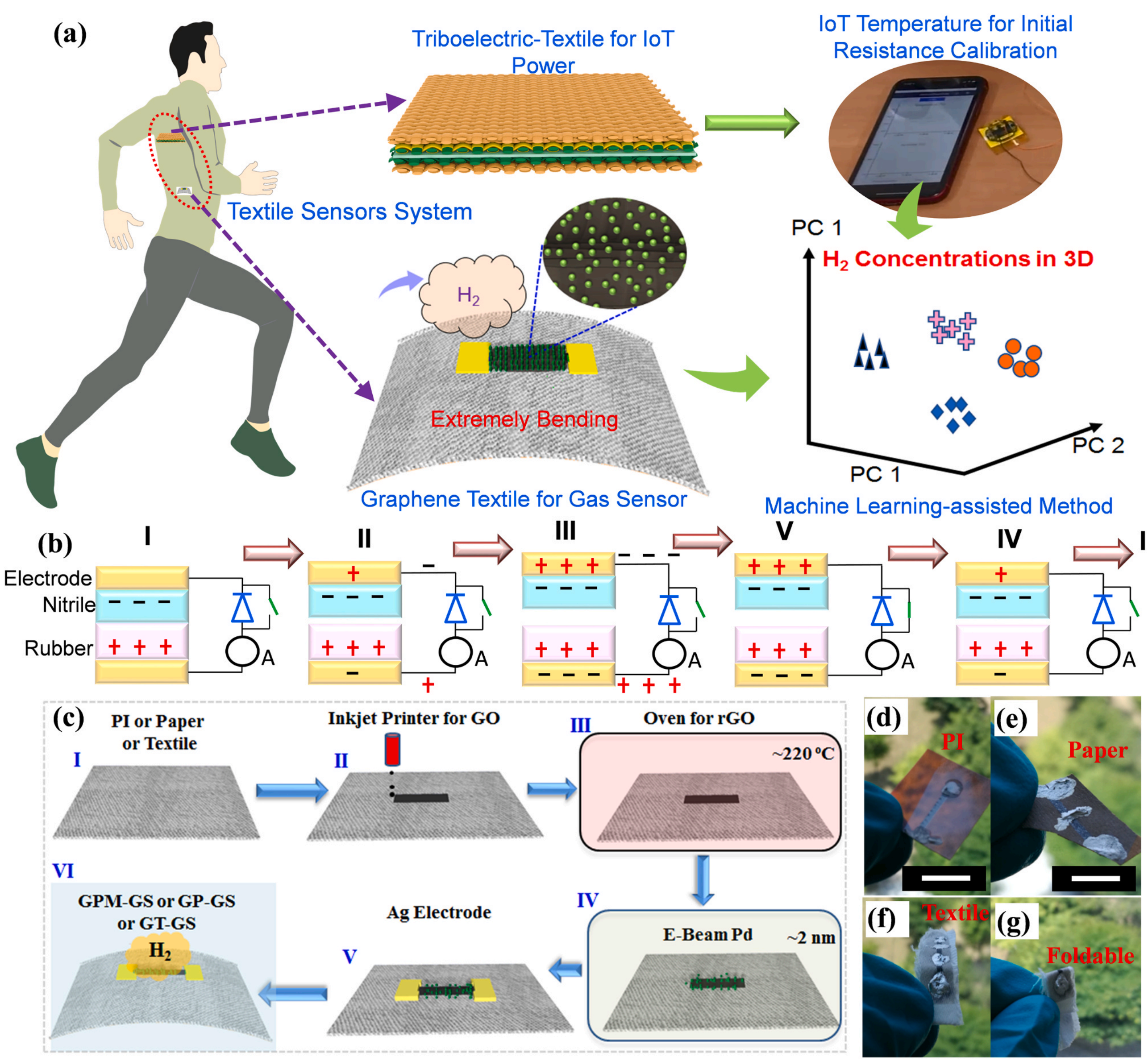

Fig. 1. (a) The machine learning-PCA method for all textile-based system by both triboelectric-textile to power sensor nodes (humidity and temperature) and textile graphene gas sensor in extreme deformed environment. (b) The principle of triboelectric effect of triboelectric-textile. (c) The manufacturing process of the gas sensor; (d) optical image of graphene on PI membrane gas sensor (GPM-GS), scale bar= 1 cm; (e) optical image of graphene on the paper gas sensor (GP-GS), (scale bar=1 cm); (f) optical image of GT-GS, scale bar= 1 cm; (g) a GT-GS with a foldable state, scale bar= 1 cm.

technology and triboelectric-textile as power source to power IoT (temperature and humidity for gas calibration), this study provides new insight into the superior flexibility and robust mechanical performance of rGO textile gas sensor, and the applications to wearable smart clothes for the internet of things (IoT).

2. Results and discussion

2.1. Schematic of machine learning-enabled and IoTs of gas sensor

Fig. 1a depicts the schematic of all textile-based system by both triboelectric-textile to power sensor nodes (humidity and temperature) and textile graphene gas sensor in extreme deformed environment. The triboelectric-textile to power IoT by human taping or normal walking, the working mechanism is based on triboelectric effect for environmental humidity and temperature sensing as a self-sustainable system [68]. The working principle of the triboelectric-textile is illustrated in Fig. 1b. The high-voltage diode is used for charge accumulation, and the switch is only closed for a short period after releasing from the triboelectric-textile. The triboelectric-textile and switch are individually controlled. As the triboelectric-textile is pressed, the negative and positive charges are generated on the contact surfaces. While releasing, negative charges tend to accumulate on the bottom electrode to compensate the negative charges on the nitrile, and, at the same time, the positive inductive charges likewise accumulate on the top electrode. The charge transfer between the two electrodes is prohibited by the high-voltage diode. The environment temperature was measured by a temperature sensor which was integrated into a bluetooth module on the cloth. The temperature fluctuation (body/clothes surface) unavoidably affects the device performance. However, the average value of the temperature was chosen for further machine learning based calibration. As shown in Fig. S1, the triboelectric-textile provided power to charge capacitor until it was full. With switch on, the charges from capacitor drove the bluetooth module to send the temperature data to the cell phone. The triboelectric-textile was used to power bluetooth wireless network for temperature and humidity, where the initial resistance from the graphene gas sensor was calibrated by the temperature and humidity from the environment. Notably, the humidity effect is less than 4% for graphene based resistive-type sensor, whereas the graphene's resistance would change a lot with different temperatures (4–5 times from room temperature to 150 ^{0}C). Accordingly, the change of resistance of our device to different humidity can be assumed to be negligible as compared to the temperature effect [69,70]. Fig. 1c depicts the fabrication process of the rGO gas sensor on three different substrates; a graphene-on-PI membrane gas sensor (GPM-GS), a graphene-on-paper gas sensor (GP-GS) and a graphene-on-textile gas sensor (GT-GS). The rGO pattern was created using the inkjet-printing process, which provided the advantages of the compatibility with various substrates, the capability of non-contact patterning and cost-effectiveness. The inkjet-printing process allows facile patterning of rGO based H_2 sensors

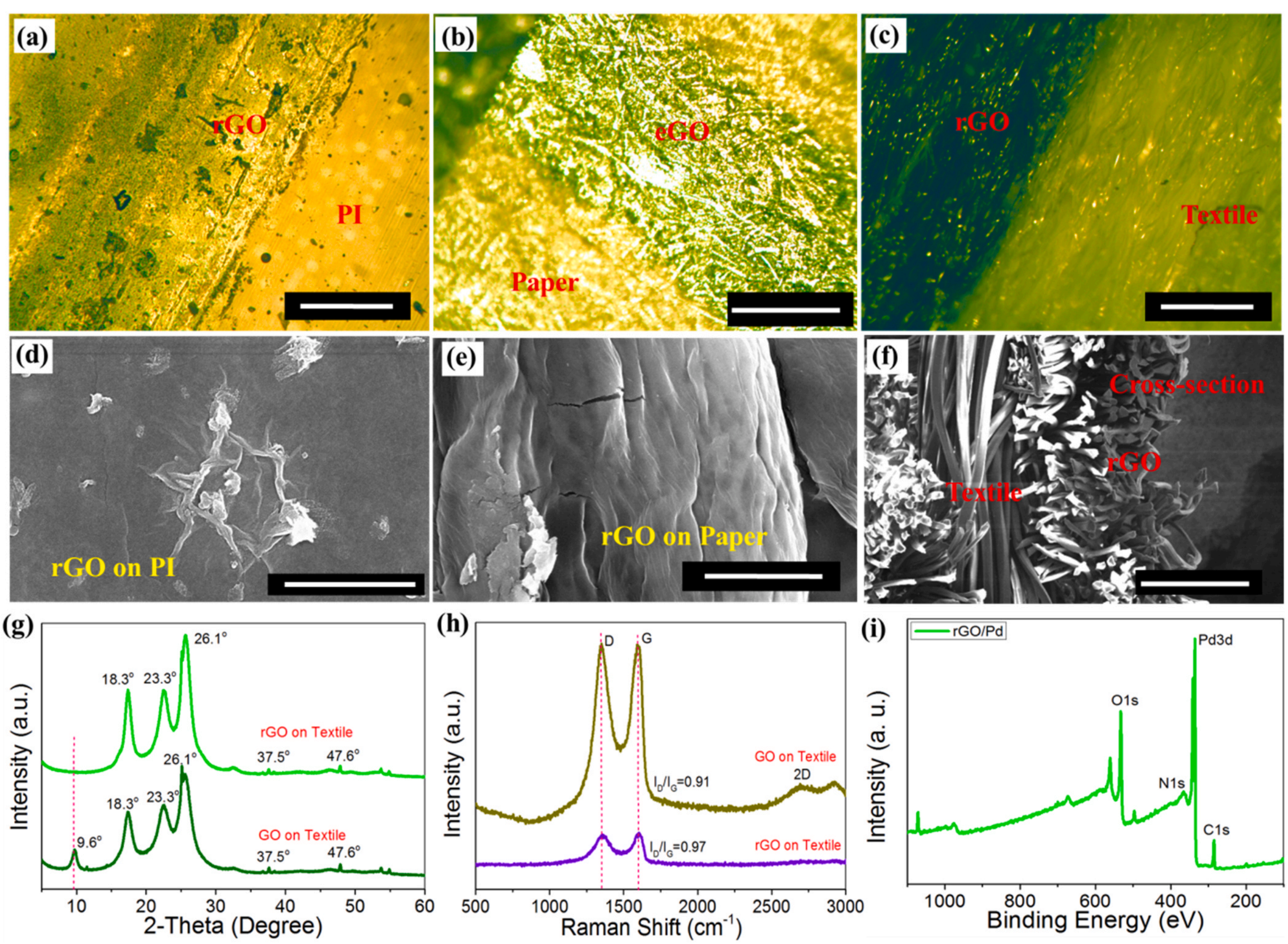

Fig. 2. Surface morphology of rGO material and materials characrization; (a) an optical microscope view of rGO on PI, scale bar= 500 μm; (b) an optical microscope view of rGO on paper, scale bar= 500 μm; (c) an optical microscope view of rGO on textile, scale bar= 500 μm; (d) SEM of rGO on PI, scale bar= 2 μm; (e) SEM of rGO on paper, scale bar= 5 μm; (f) SEM of the cross-section of rGO on a textile substrate, scale bar= 500 μm. (g) a wide-angle XRD of GO and rGO; (h) Raman spectra; (i) a wide XPS scan of graphene with Pd NPs.

with arbitrary patterns as shown in Fig. S2. Inkjet printing patterns for GP-GS is shown in Video S1 in Supporting information. The optical images of the fabricated sensors are presented in Fig. 1d-f, and the foldable state of the GT-GS is depicted in Fig. 1g. Fig. 1c illustrates the schematic of Pd NPs coated on the rGO/polyester microfibers in the GT-GS. Detailed information on the Pd NPs on rGO/polyester microfibers can be found in Fig. S3. The gas sensor can be sewn on or attached to a commercial cloth to form a wearable device on textiles for IoT applications in extreme deformed environment.

Supplementary material related to this article can be found online at doi:10.1016/j.nanoen.2021.106035.

2.2. Material characterization and analysis

Microstructures of fabricated rGO sensors were investigated by observing optical and SEM images. Fig. 2a-c depict the surface morphology of the coated rGO on three different substrates using an optical microscope, and the clearer surface morphologies using a scanning electron microscope (SEM) are shown in Fig. 2d and Fig. S4b. The figures confirm that both the porous paper microfiber substrate and the textile microfiber substrate have much larger surface areas than the PI flat membrane substrate due to the 3D porous microstructure of the microfibers. The analysis also confirmed that the porous paper microfiber contributed more 3D microstructure wrinkles than the textile microfiber. Meanwhile, GT-GS with textile was observed a good mechanic robust than the GP-GS with porous paper. Fig. 2f and Fig. S4a clearly show the cross-section of the coated rGO on a textile substrate with a thickness of 50–100 μm using the inkjet printing. Fig. S4c is a magnified top view of the graphene textile. Fig. 2g describes the X-ray diffraction (XRD) of the graphene with an intense peak centered at $2\theta = 9.6^{\circ}$, which is in agreement with heavily oxidized rGO materials. Fig. 2h depicts the Raman spectroscopy of rGO on textiles with three prominent peaks: the D peak 1368 cm^{-1} is called the "defect-related" peak, the G peak 1592 cm^{-1} is related to the E2g phonon of graphene, and the 2D peak originates in the second-order phonon. The value of I_D/I_G increased from 0.91 to 0.97, which demonstrated deoxidation from GO to rGO. The X-ray photoelectron spectroscopy (XPS) measurements of the sensing materials were performed to investigate further findings as shown in Fig. 2i and Fig. S5. The high-resolution spectra of the C1s peaks are shown with four components, namely, C–C (283.5 eV), C–O (285.3 eV), C=O (286.7 eV) and O-C=O (291.2 eV) as shown in Fig. S5b. The XPS spectra of the Pd3d regions of Pd on the rGO on the textile are shown in Fig. S5c. The $Pd3d_{5/2}$ states with 334.6 eV and $Pd3d_{3/2}$ states with 340.2 eV indicate a small positive value relative to pure polycrystalline Pd interaction upon the formation of an intermetallic compound. The O1s spectra and N1s spectra of XPS are shown in Fig. S6a and Fig. S6b, respectively. The characterizations of the energy-dispersive X-ray spectroscopy (EDS) of the rGO with and without Pd nanoparticles (NPs) on a textile substrate are shown in Fig. S7. These results revealed the wrinkled microstructure pattern of the rGO coated on the textile.

2.3. Working mechanism and environment measurement

Fig. S8a gives a schematic of the rGO on the surface of 3D textile microfibers, and Fig. S8b shows an SEM image of the rGO/Pd textile microfiber. The rGO defects (e.g., the O atoms) were due to the adsorption of gas molecules, which significantly altered the electrical conduction characteristics of graphene/Pd during the process of H_2 exposure [1]. The schematic of the atoms of the GO, rGO and rGO with Pd are shown in Figs. S8c–e. When the H_2 gas reacted with the Pd NPs, the resistance of the rGO with Pd changed due to the adsorption and desorption of the nonpolar H_2 molecules. H_2 was incorporated into the Pd lattice in the form of PdH_x, which lowered the work function of Pd and created a transfer of electrons from the NP to the graphene underneath [3]. The response and recovery of the gas sensor were determined by recording the resistance change by the exposure to different H_2 concentrations. To evaluate the gas sensing performance, we described the response (S) of the sensor as follows:

$$S = \frac{R - R_0}{R_0} \times 100\% \quad (1)$$

where R_0 and R represent the initial resistance and the resistance recorded after the gas sensor was exposed to H_2, respectively.

To investigate the electronic properties of rGO/Pd textile and rGO/Pd PI devices, their current-voltage (I-V) characteristics were obtained as shown in Figs. S9a-b. The conductance of the rGO/Pd device displayed a linear ohmic characteristic. Furthermore, we investigated the consistency of sensor responses of fabricated GPM-GS, GP-GS and GT-GS under different sets of input voltages. Fig. 3a-c depict the sensor response to different concentrations of H_2, and Fig. S10 show reasonable consistency in the sensor response regardless of the input voltage for the concentration range of 0.06%−1.3%. The working lifetime of the gas sensor could be very long because of no mechanical damage. We set the different hydrogen concentrations with different time segments with/without hydrogen by a computer controller. Hydrogen sensing using GT-GS is shown in Video S2 in Supporting information. When the H_2 concentration increased or decreased, it caused the current changes due to the structural changes in atoms in the graphene/Pd during the process of adsorption or desorption of H_2. During H_2 detection, the nonpolar H_2 molecules interacted with Pd NPs on the surface of the rGO coated on the 3D microstructure of microfibers. Fig. 3d shows the comparison of sensor performance to H_2 exposure. We found that GP-GS and GT-GS had around six times higher sensor response than GPM-GS due to the 3D porous microstructures of the microfibers. Because of more wrinkled 3D microstructures of microfibers on the porous paper than on the textile substrate, we obtained relatively larger sensor responses for GP-GS than for GT-GS. However, the fragility of the paper substrate constrained the practical applications of GP-GS as compared to GT-GS with good mechanical flexibility and foldability as shown in Video S3 and Video S4 in Supporting information. In addition, Fig. 3e shows the repeated H_2 exposure experiments of GT-GS to demonstrate the good repeatability of our device. In determining the gas response with/without Pd on rGO of the three devices, the flat curves in Fig. 3f and Fig. S11 represent that the rGO without Pd decoration had no response to the H_2 exposure during the entire gas sensing experiments. This result reflects that the response of rGO to H_2 is activated by Pd decoration on its surface. It confirms that the gas response is only from the change of hydrogen concentrations by our observation (the comparison between the flat curve and gas response curve). Fig. 3g–i and Figs. S12–S13 show the temperature influence analysis of the GT-GS. We observed that high temperature resulted in higher current flow through our device, meaning that the high temperatures resulted in a resistance decrease in our gas sensor device. Thus, the initial resistance from graphene textile gas sensor is strongly related with temperature, which means the textile-triboelectric to power IoT for temperature is a key for initial resistance calibration of graphene textile gas sensor during the H_2 sensing. By investigating the gas responses of the GT-GS under different sets of temperatures, we found that high temperature dramatically reduced the H_2 response of our gas sensor device as shown in Fig. 3h and 3i and Fig. S14. Notably, the measurement conditions were the same except the change of the temperature for each test set. For example, when the temperature increased from room temperature (RT) to 120 °C, the response of GT-GS decreased from about 15% to about 6% for 4000 ppm of H_2 gas. Moreover, we observed that the response time was about 1.5 times shorter than its recovery time, but interestingly the temperature did not affect the time too much (about 20% difference) as shown in Fig. S14. The response time and the recovery time in our case were calculated as 80% of the resistance changes during the H_2 gas measurement.

Supplementary material related to this article can be found online at doi:10.1016/j.nanoen.2021.106035.

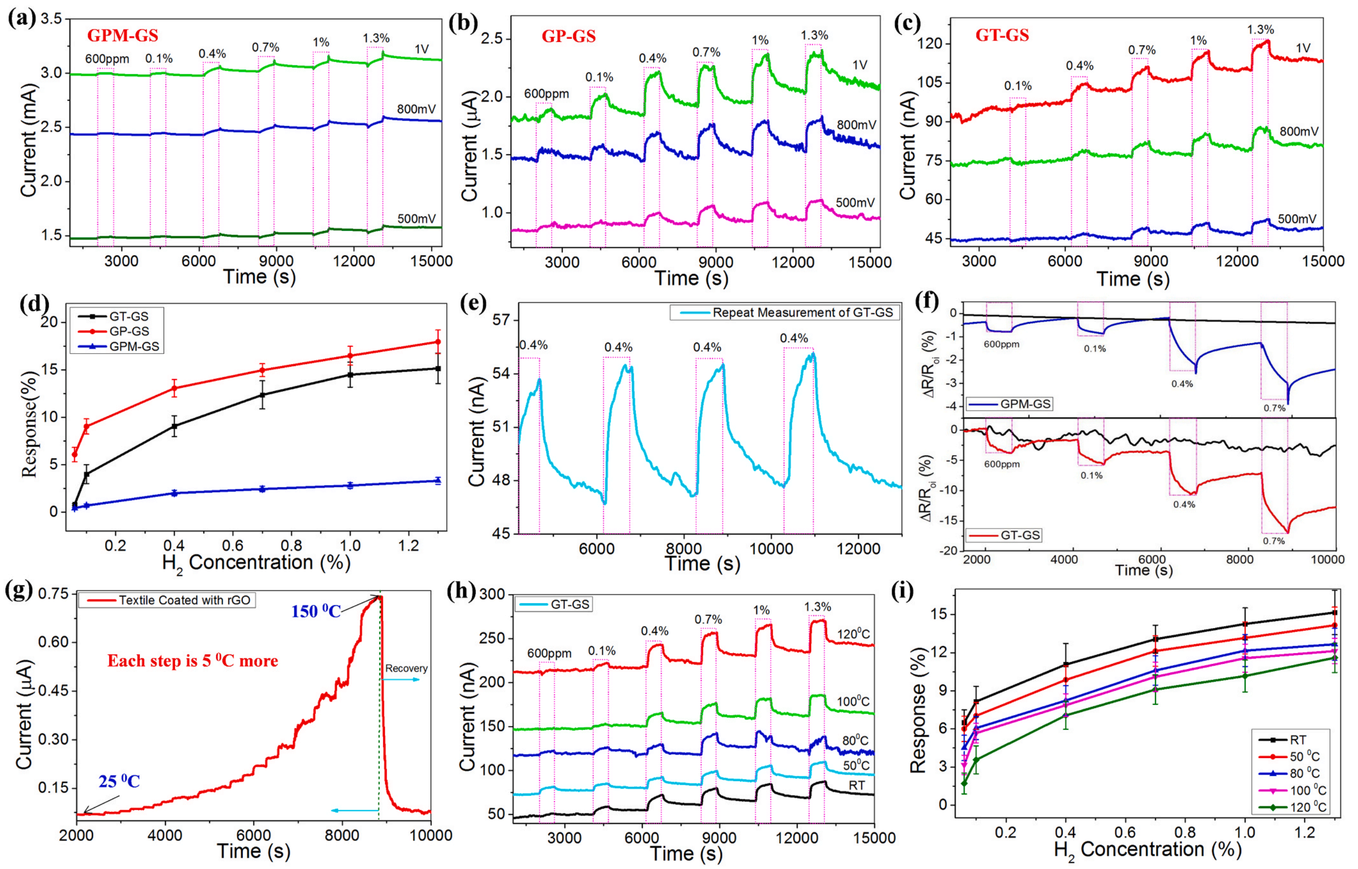

Fig. 3. The gas response under different sets of input voltages for (a) GPM-GS, (b) GP-GS, and (c) GT-GS. (d) response vs. H_2 concentrations for different gas sensors under bias of 1 V. (e) gas response of GT-GS to the repeated 4000 ppm H_2 exposure. (f) H_2 gas response of the GPM-GS, GP-GS, and GT-GS, the device initial resistance R_{Oi} in the diagram was used for a better gas response observation with/without Pd NPs. (g) Temperature influence analysis of the GT-GS. (h) H_2 gas response at different sets of temperatures. (i) Response vs. H_2 concentrations at different sets of temperatures. It was observed almost 60% better response at room temperature than 120 ^{0}C.

2.4. Extremely deformable test and its robust mechanical performance

To demonstrate the mechanical flexibility of GT-GS, we conducted gas tests in different sets of bending deformed states as shown in Fig. 4a, and the normalized resistance changed for different sets of bending states as shown in Fig. 4b. The test confirmed that the devices worked well under those bending deformations. The coefficient of variance (CoV) of the developed Pd/graphene-based device was calculated for the different H_2 concentrations as shown in Table S1. CoV was calculated by taking the ratio of the standard deviation to the average response magnitudes of the sensor toward each hydrogen concentration [71]. Fig. 4c-d show the feasibility of the GT-GS H_2 detection on a flat membrane, a glove and a piece of clothing. Furthermore, the foldable measurement of GT-GS and its bending conditions are shown in Fig. 4e, which demonstrates its H_2 sensing capability in folding situations. The graphene textile H_2 sensor was placed in the gas chamber with foldable status for the H_2 measurement. Fig. S15 shows the reliability of GT-GS because there was no evident degradation after a long-term observation (a month). The mechanical durability of the H_2 sensor is demonstrated in Fig. S16, which shows before and after 10,000 times bending. Thus, we confirmed that GT-GS has sufficient mechanical robustness. Table S2 in Supplementary Information shows the comparison of the advantages of the graphene textile H_2 sensor presented in our study and other existing state-of-the-art H_2 sensors. Compared to the current existing graphene H_2 sensors in references [8,26,29,32,34,42], our H_2 sensors show much higher response. In addition, we confirmed that GT-GS possesses much better flexibility and foldability than other devices introduced in the literature.

2.5. IoT for environment parameters and machine learning-enabled gas sensing

The charging and discharging curve by triboelectric-textile to power IoT were as shown in Fig. 5a [65], where each voltage drops from ~8 V to ~2.7 V representing a discharging to the bluetooth module. Here, the charging and discharging curves with bluetooth module was driven by triboelectric-textile to power IoT for temperature and humidity, the temperature was used to calibrate the initial resistance from graphene textile H_2. To meet the extreme deformed environment for H_2 detection, machine learning is a useful tool for a better and clear identification of the gas sensing based on raw data. PCA is mostly used as a tool in exploratory data analysis and for making predictive models as shown in Fig. 5b. It noted that the raw data by the PCA was obtained from Fig. 3b (flat under 3 V) and Fig. 4a (three bending conditions under 1 V) However, the curves in these two figures are not easy for human beings to identify the real concentration of the exposure gas. To visualize the results by the machine learning tool of PCA, the obtained raw data from these two figures can be well handled to identify the H_2 concentrations. Each concentration was decoupled to be a data point in 2 dimensions space or 3 dimensions space. The 2D cluster data based on PCA was shown in Fig. 5c. Thus, the concentrations can be well identified based on the PCA using the cluster dots. To increase the accuracy using the PCA, the modified method based on the 3D was demonstrated as shown in Fig. 5d. The result shows that the concentrations of H_2 concentrations can be well demonstrated.

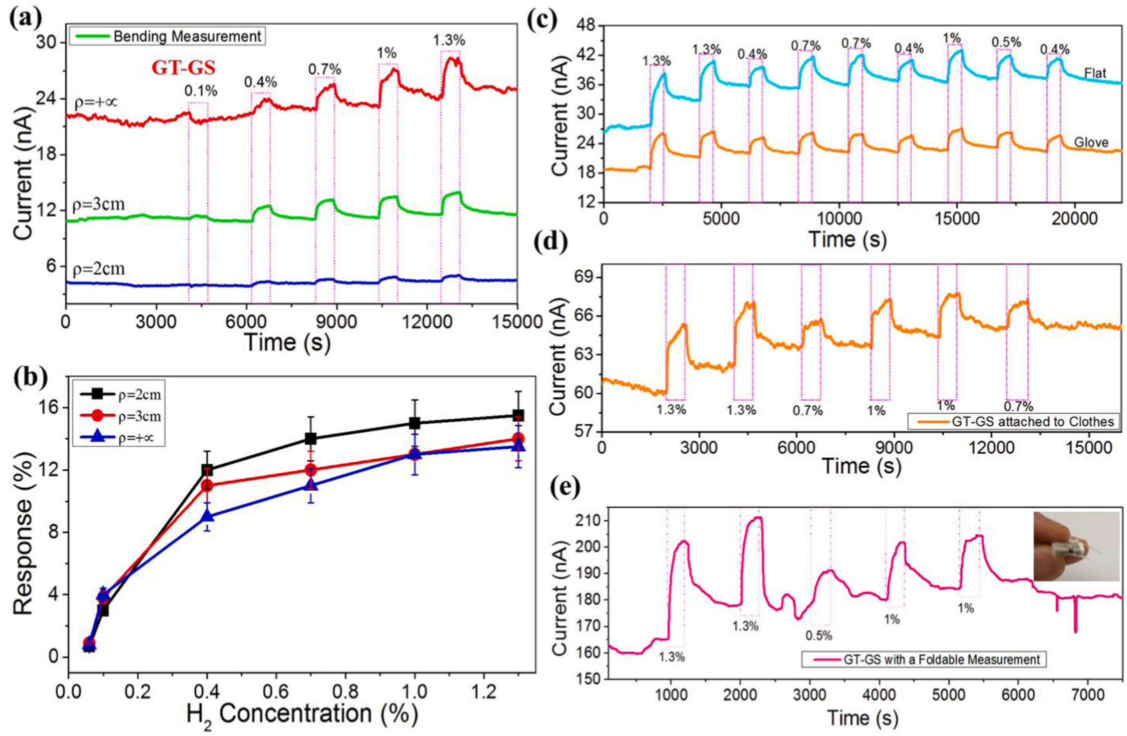

Fig. 4. (a) Response of the GT-GS to H_2 gas, without bending, with a bending radius of 3 cm, and with a bending radius of ~2 cm. (b) Response vs. H_2 concentration with different sets of bending states. (c) GT-GS with random gas concentration measurements in a flat state or on a glove, bending radius ~3 cm. (d) GT-GS was measured on a cloth substrate with random H_2 concentration exposure, bending radius + ∞. (e) Another GT-GS measurement with a foldable state, bending radius ~0 cm.

3. Conclusions

This study demonstrated a flexible and foldable H_2 sensing using inkjet-printed reduced graphene oxide (rGO) on textile substrate for applications in wearable smart clothes. Inkjet printing allowed facile and fast patterning of rGO materials on various flexible substrates. We found that the GT-GS had about six times higher H_2 sensing response than the GPM-GS in a concentration range of 1000 ppm to 1%. The temperature factor analysis of the GT-GS demonstrated a 60% higher H_2 response at RT than at 120 °C. With the machine learning-enabled PCA technology and triboelectric-textile as power source to power IoT (temperature and humidity for gas calibration), the random H_2 concentration tests and wearable applications in smart clothes not only demonstrated a robust mechanical performance for the GT-GS but also good flexibility and foldability. Furthermore, this study of H_2 sensors provides a deep understanding of the 3D foldable inkjet-printed graphene textile, and it demonstrates the applications in wearable application with the machine learning-enabled for the IoT.

4. Experimental section

4.1. Fabrication of graphene gas sensor

The printing system is the Dimatix 2831 Materials Printer from Fujifilm Company. As shown in Figs. S2a, Fig. 1e–f, GO solution (dispersion in H_2O 4 mg/mL) from Sigma-Aldrich can be printed onto various substrates (such as porous paper microfiber) with any patterns. The patterned GO device was placed into an oven at 220 °C for 5 h to produce rGO with the air pressure. GO was then reduced (rGO) via chemical or thermal treatments to recover the desired properties of graphene such as electrical conductivity. The morphological difference between the GO and the rGO can be identified as shown in Figs. S2b and S2c in Supporting Information. To make the produced rGO sensitive to H_2, Pd NPs were coated onto the surface of the device using e-beam evaporation with a thickness of about 2 nm. Finally, a silver paste was applied to two terminals of the rGO film as metal electrodes.

4.2. Material characterization

The surface morphologies of the GO and rGO were characterized by scanning electron microscope (SEM, SIRON-100, FEI Corp., Netherlands). The X-ray photoelectron spectroscopy and X-ray diffraction of the fabricated materials were performed by K-alpha XPS System (Thermo VG Scientific, USA) and D/MAX-2500 XRD System (RIGAKU Company, Japan), respectively. The Raman spectroscopy was measured using equipment LabRAM HR Evolution (HORIBA France SAS company, France).

4.3. Gas sensing equipment and measurement

Fig. S17 (Supporting Information) depicts the setup for H_2 gas sensing measurements. Three mass flow controllers (MFCs) were connected to the gas measurement chamber to provide the inlet gases. The ratio and flow rate of gases including H_2, N_2, and O_2 were accurately controlled using MFCs. H_2 in the carrier gases were injected into the gas measurement chamber through a mixer joint. Two signal wires in the chamber were used to connect the rGO based gas sensors on a homemade probe station. The probe station was made from two copper probes and a substrate holder to connect the sensor with a source meter Keithley 2400B (Tektronix, USA) and Keithley 2635B (Tektronix, USA). The H_2 sensing characteristics of the gas sensor were measured using this two-probe system with the source meter to record the resistance change. A computer was used to control the MFCs and collect the measurement data automatically.

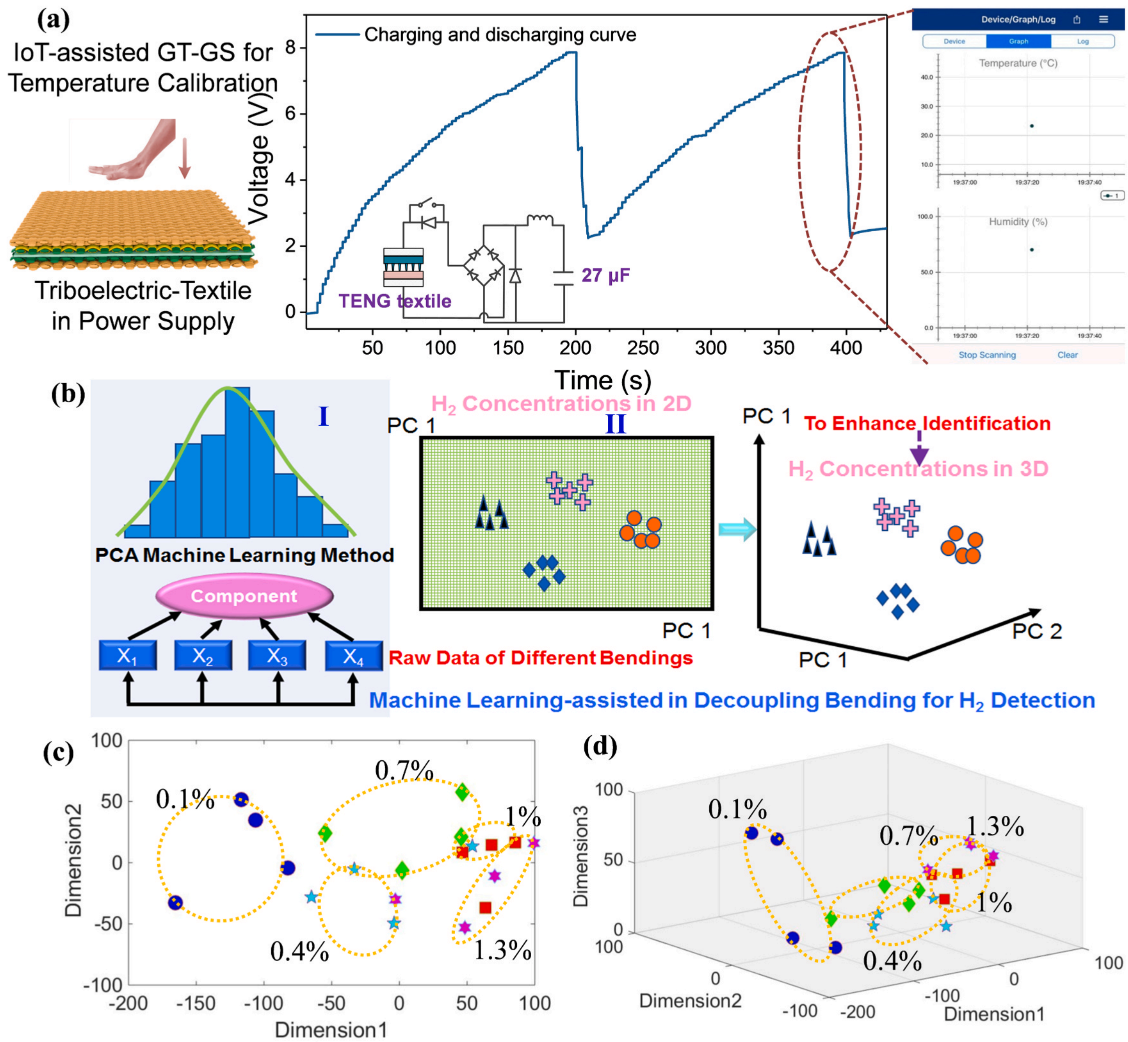

Fig. 5. (a) Charging and discharging curves with bluetooth module driven triboelectric textile to power IoT for temperature and humidity, the temperature was used to calibrate the initial resistance from graphene textile for H_2. (b) Machine learning-PCA method for extreme deformed environment in 2D and 3D for better visualization identification. (c) Extreme deformed environment in 2D for visualization, and (d) in 3D.

CRediT authorship contribution statement

The manuscript was written through contributions of all authors. The concept was proposed by Dr. Jianxiong Zhu and Dr. Minkyu Cho. The experiments were performed by Dr. Jianxiong Zhu, Dr. Minkyu Cho, Junseong Ahn, Jaeho Park, and Tianyiyi He. The conceptualization was discussed and designed by Yutao Li, Dr. Jianxiong Zhu, and Prof. Tian-Ling Ren. The funding and the entire concept design were supported by Prof. Inkyu Park and Prof. Chengkuo Lee. All authors have given approval to the final version of the manuscript.

Declaration of Competing Interest

The authors declare that they have no known competing financial interests or personal relationships that could have appeared to influence the work reported in this paper.

Acknowledgments

J. Zhu, and M. Cho contributed equally to this work. This work was supported by Multi-Ministry Collaborative Research and Development Program (Development of Techniques for Identification and Analysis of Gas Molecules to Protect Against Toxic Substances) (NRF-2017M3D9A1073863) and National Research Foundation of Korea (NRF) grant funded by the Korea government (MSIT) (No. 2021R1A2C3008742).

Appendix A. Supporting information

Supplementary data associated with this article can be found in the online version at doi:10.1016/j.nanoen.2021.106035.

References

[1] A. Singhal, H. Charaya, I. Lahiri, Noble metal decorated graphene-based gas sensors and their fabrication: a review, Crit. Rev. Solid State Mater. Sci. 42 (2017) 499–526.

[2] J. Lee, J. Oh, J. Jun, J. Jang, Wireless hydrogen smart sensor based on Pt/graphene-immobilized radio-frequency identification tag, ACS Nano 9 (2015) 7783–7790.

[3] K. Toda, R. Furue, S. Hayami, Recent progress in applications of graphene oxide for gas sensing: a review, Anal. Chim. Acta 878 (2015) 43–53.

[4] J. Lim, N. Phiboolsirichit, S. Mubeen, M. Deshusses, A. Mulchandani, N. Myung, Electrical and gas sensing properties of polyaniline functionalized single-walled carbon nanotubes, Nanotechnology 21 (2010), 075502.

[5] A. Smith, K. Elgammal, X. Fan, M. Lemme, A. Delin, M. Rasander, L. Bergqvist, S. Schröder, A. Fischer, F. Niklaus, M. Ostling, Graphene-based CO_2 sensing and its cross-sensitivity with humidity, RSC Adv. 7 (2017) 22329–22339.

[6] Z. Zhan, G. Zheng, W. Tao, Y. Cai, D. Sun, D. Wu, Electrohydrodynamic impulse printing PANI sensor for NH_3 gas, Proc. Inst. Mech. Eng. Part N J. Nanoeng. Nanosyst. 226 (2012) 9–13.

[7] G. Behzadipour, L. Fekriaval, Highly sensitive work function hydrogen gas sensor based on PdNPs/SiO_2/Si structure at room temperature, Results Phys. 7 (2017) 1993–1999.
[8] M. Shafiei, P. Spizzirri, R. Arsat, J. Yu, J. Plessis, S. Dubin, R. Kaner, K. Kalantar-zadeh, W. Wlodarski, Platinum/graphene nanosheet/SiC contacts and their application for hydrogen gas sensing, J. Phys. Chem. C. 114 (2010) 13796–13801.
[9] A. Uddin, G. Chung, A self-powered active hydrogen gas sensor with fast response at room temperature based on triboelectric effect, Sens. Actuators B: Chem. 231 (2016) 601–608.
[10] U. Latif, F. Dickert, Graphene hybrid materials in gas sensing applications, Sensors 15 (2015) 30504–30524.
[11] G. Naik, S. Krishnaswamy, Room-temperature humidity sensing using graphene oxide thin films, Graphene 5 (2016) 1–13.
[12] Y. Peng, J. Ye, L. Zheng, K. Zou, The hydrogen sensing properties of Pt–Pd/reduced graphene oxide based sensor under different operating conditions, RSC Adv. 6 (2016) 24880–24888.
[13] C. Piloto, M. Notarianni, M. Shafiei, E. Taran, D. Galpaya, C. Yan, N. Motta, Highly NO_2 sensitive caesium doped graphene oxide conductometric sensors, Beilstein J. Nanotechnol. 5 (2014) 1073–1081.
[14] X. Yu, H. Cheng, M. Zhang, Y. Zhao, L. Qu, G. Shi, Graphene-based smart materials, Nat. Rev. Mater. 2 (2017) 17046.
[15] E. Singh, M. Meyyappan, H. Nalwa, Flexible graphene-based wearable gas and chemical sensors, ACS Appl. Mater. Interfaces 9 (2017) 34544–34586.
[16] S. Wang, N. Liu, J. Su, L. Li, F. Long, Z. Zou, X. Jiang, Y. Gao, Highly stretchable and self-healable supercapacitor with reduced graphene oxide based fiber springs, ACS Nano 11 (2017) 2066–2074.
[17] T. Wang, D. Huang, Z. Yang, S. Xu, G. He, X. Li, N. Hu, G. Yin, D. He, L. Zhang, A review on graphene-based gas/vapor sensors with unique properties and potential applications, Nano Micro Lett. 8 (2015) 95–119.
[18] D. Wu, L. Wu, H. Cui, H. Zhang, J. Yu, A rapid ammonia sensor based on lysine nanogel-sensitized PANI/PAN nanofibers, J. Mater. Chem. B 4 (2016) 1520–1527.
[19] J. Wu, K. Tao, Y. Guo, Z. Li, X. Wang, Z. Luo, S. Feng, C. Du, D. Chen, J. Miao, L. Norford, A 3D chemically modified graphene hydrogel for fast, highly sensitive, and selective gas sensor, Adv. Sci. 4 (2017), 1600319.
[20] Z. Xu, K. Wu, S. Zhang, Y. Meng, H. Li, L. Li, Highly sensitive airflow sensors with an ultrathin reduced graphene oxide film inspired by gas exfoliation of graphite oxide, Mater. Horiz. 4 (2017) 383–388.
[21] W. Yuan, G. Shi, Graphene-based gas sensors, J. Mater. Chem. A 1 (2013) 10078–10091.
[22] X. Zhang, H. Cui, Y. Gui, Synthesis of graphene-based sensors and application on detecting SF6 decomposing products: a review, Sensors 17 (2017) 363.
[23] B. Chu, J. Nicolosi, C. Lo, W. Strupinski, S. Pearton, F. Ren, Effect of coated platinum thickness on hydrogen detection sensitivity of graphene-based sensors, Electrochem. Solid-State Lett. 14 (2011) K43–47.
[24] N. Eom, H. Cho, Y. Song, W. Lee, T. Sekino, Y. Choa, Room-temperature H_2 gas sensing characterization of graphene-doped porous silicon via a facile solution dropping method, Sensors 17 (2017) 1–7.
[25] S. Fardindoost, S. Hatamie, A. Zad, F. Astaraei, Hydrogen sensing properties of nanocomposite graphene oxide/Co-based metal organic frameworks (Co-MOFs@GO), Nanotechnology 29 (2018), 015501.
[26] N. Ha, C. Long, N. Nam, N. Hue, N. Phuong, H. Hong, Characteristics of hydrogen sensor based on monolayer of Pt nanoparticles decorated on single-layer graphene, J. Electron. Mater. 46 (2017) 3353–3358.
[27] J. Hong, S. Lee, J. Seo, S. Pyo, J. Kim, T. Lee, A highly sensitive hydrogen sensor with gas selectivity using a PMMA membrane-coated Pd nanoparticle/single-layer graphene hybrid, ACS Appl. Mater. Interfaces 7 (2015) 3554–3561.
[28] J. Johnson, A. Behnam, S. Pearton, A. Ural, Hydrogen sensing using Pd-functionalized multi-layer graphene nanoribbon networks, Adv. Mater. 22 (2010) 4877–4880.
[29] A. Kaniyoor, R. Jafri, T. Arockiadoss, S. Ramaprabhu, Nanostructured Pt decorated graphene and multi walled carbon nanotube based room temperature hydrogen gas sensor, Nanoscale 1 (2009) 382–386.
[30] R. Paul, S. Badhulika, N. Saucedo, A. Mulchandani, Graphene nanomesh as highly sensitive chemiresistor gas sensor, Anal. Chem. 84 (2012) 8171–8178.
[31] A. Lipatov, A. Varezhnikov, P. Wilson, V. Sysoev, A. Kolmakov, A. Sinitskii, Highly selective gas sensor arrays based on thermally reduced graphene oxide, Nanoscale 5 (2013) 5426–5434.
[32] O. Lupan, V. Postica, M. Mecklenburg, K. Schulte, Y. Mishra, B. Fiedler, R. Adelung, Low powered, tunable and ultra-light aerographite sensor for climate relevant gas monitoring, J. Mater. Chem. A 4 (2016) 16723–16730.
[33] R. Lv, G. Chen, Q. Lie, A. McCreary, A. Botello-Méndezf, S. Morozovg, L. Liangh, X. Declerckf, N. Perea-López, D. Culleni, S. Feng, A. Elías, R. Cruz-Silvaj, K. Fujisawa, M. Endoj, F. Kang, J. Charlierf, V. Meunierh, M. Pank, A. Harutyunyan, K. Novoselov, M. Terronesb, Ultrasensitive gas detection of large-area boron-doped graphene, PNAS 19 (2016) 14527–14532.
[34] U. Lange, T. Hirsch, V. Mirsky, O. Wolfbeis, Hydrogen sensor based on a graphene–palladium nanocomposite, Electrochim. Acta 56 (2011) 3707–3712.
[35] F. Rigoni, R. Maiti, C. Baratto, M. Donarelli, J. MacLeod, B. Gupta, M. Lyu, A. Ponzoni, G. Sberveglieri, N. Motta, G. Faglia, Transfer of CVD-grown graphene for room temperature gas sensors, Nanotechnology 28 (2017), 414001.
[36] S. Some, Y. Xu, Y. Kim, Y. Yoon, H. Qin, A. Kulkarni, T. Kim, H. Lee, Highly sensitive and selective gas sensor using hydrophilic and hydrophobic graphenes, Sci. Rep. 3 (2013) 1868.
[37] T. Sun, Z. Zhang, J. Xiao, C. Chen, F. Xiao, S. Wang, Y. Liu, Facile and green synthesis of palladium nanoparticles-graphene-carbon nanotube material with high catalytic activity, Sci. Rep. 3 (2013) 2527.
[38] Z. Abideen, H. Kim, S. Kim, An ultra-sensitive hydrogen gas sensor using reduced graphene oxide-loaded ZnO nanofibers, Chem. Commun. 51 (2015) 15418–15421.
[39] A. Venkatesan, S. Rathi, I. Lee, J. Park, D. Lim, G. Kim, E. Kannan, Low temperature hydrogen sensing using reduced graphene oxide and tin oxide nanoflowers based hybrid structure, Semicond. Sci. Technol. 31 (2016), 125014.
[40] G. Reddy, P. Raghavendra, P. Chandana, L. Sarma, Halide-aided controlled fabrication of Pt–Pd/graphene bimetallic nanocomposites for methanol electrooxidation, RSC Adv. 5 (2015) 100522–100530.
[41] Z. Zhang, X. Zou, L. Xu, L. Liao, W. Liu, J. Ho, X. Xiao, C. Jiang, J. Li, Hydrogen gas sensor based on metal oxide nanoparticles decorated graphene transistor, Nanoscale 7 (2015) 10078–10084.
[42] X. Chen, F. Yasin, P. Eggers, R. Boulos, X. Duan, R. Lamb, K. Lyer, C. Raston, Non-covalently modified graphene supported ultrafine nanoparticles of palladium for hydrogen gas sensing, RSC Adv. 3 (2013) 3213.
[43] I. Kang, H. So, G. Bang, J. Kwak, J. Lee, W. Ahn, Recovery improvement of graphene-based gas sensors functionalized with nanoscale heterojunctions, Appl. Phys. Lett. 101 (2012), 123504.
[44] B. Ando, S. Baglio, A. Bulsara, T. Emery, V. Marletta, A. Pistorio, Low-cost inkjet printing technology for the rapid prototyping of transducers, Sensors 17 (2017) 1–11.
[45] L. Huang, Y. Huang, J. Liang, X. Wan, Y. Chen, Graphene-based conducting inks for direct inkjet printing of flexible conductive patterns and their applications in electric circuits and chemical sensors, Nano Res. 4 (2011) 675–684.
[46] Y. Seekaew, S. Lokavee, D. Phokharatkul, A. Wisitsoraat, T. Kerdcharoen, C. Wongchoosuk, Low-cost and flexible printed graphene–PEDOT: PSS gas sensor for ammonia detection, Org. Electron. 15 (2014) 2971–2981.
[47] G. Mattana, D. Briand, Recent advances in printed sensors on foil, Mater. Today 19 (2016) 88–99.
[48] J. Zheng, J. Diao, Y. Jin, A. Ding, B. Wang, B. Weng, J. Chen, An inkjet printed Ti_3C_2-GO electrode for the electrochemical sensing of hydrogen peroxide, J. Electrochem. Soc. 165 (5) (2018) B227–B231.
[49] I. Cho, Y. Sim, M. Cho, Y. Cho, I. Park, Monolithic micro light-emitting diode/metal oxide nanowire gas sensor with microwatt-level power consumption, ACS Sens. 5 (2) (2020) 563–570.
[50] M. Cho, J. Zhu, H. Kim, K. Kang, I. Park, Half-pipe palladium nanotube-based hydrogen sensor using a suspended nanofiber scaffold, ACS Appl. Mater. Interfaces 11 (14) (2019) 13343–13349.
[51] M. Cho, J. Yun, D. Kwon, K. Kim, I. Park, High-sensitivity and low-power flexible schottky hydrogen sensor based on silicon nanomembrane, ACS Appl. Mater. Interfaces 10 (15) (2018) 12870–12877.
[52] W. Song, J. Zhu, B. Gan, S. Zhao, H. Wang, J. Li, J. Wang, Flexible, stretchable, and transparent planar microsupercapacitors based on 3D porous laser-induced graphene, Small (2017), 1702249.
[53] J. Zhu, M. Cho, Y. Li, J. Park, I. Cho, T. Ren, I. Park, I. Biomimetic turbinate-like artificial nose for hydrogen detection based on 3D porous laser-induced graphene, ACS Appl. Mater. Interfaces 11 (2019), 2724386-24394.
[54] M. Gao, M. Cho, H. Han, Y. Jung, I. Park, Palladium-decorated silicon nanomesh fabricated by nanosphere lithography for high performance, room temperature hydrogen sensing, Small 14 (2018), 1703691.
[55] B. Choi, J. Ahn, J. Lee, J. Yoon, J. Lee, M. Jeon, D. Kim, D. Kim, I. Park, S. Choi, A bottom-gate silicon nanowire field-effect transistor with functionalized palladium nanoparticles for hydrogen gas sensors, Solid State Electron. 114 (2015) 76–79.
[56] H. Eom, J. Lee, A. Pichitpajongkit, M. Amjadi, J. Jeong, E. Lee, J. Lee, I. Park, Ag@Ni core-shell nanowire network for robust transparent electrodes against oxidation and sulfurization, Small 10 (20) (2014) 4171–4181.
[57] J. Ahn, J. Yun, Y. Choi, I. Park, Palladium nanoparticle decorated silicon nanowire field-effect transistor with side-gates for hydrogen gas detection, Appl. Phys. Lett. 104 (2014), 013508.
[58] Q. Shi, Z. Zhang, T. Chen, C. Lee, Minimalist and multi-functional human machine interface (HMI) using a flexible wearable triboelectric patch, Nano Energy 62 (2019) 355–366.
[59] J. Zhu, X. Guo, D. Meng, M. Choi, I. Park, R. Huang, W. Song, A flexible comb electrode Ttriboelectric-electret nanogenerator with separated microfibers for self-powered position, motion direction and acceleration tracking sensor, J. Mater. Chem. A 6 (2018) 16548–16555.
[60] C. Qiu, F. Wu, Q. Shi, C. Lee, M. Yuce, Sensors and control interface methods based on triboelectric nanogenerator in IoT applications, IEEE Access 7 (2019) 92745–92757.
[61] J. Zhu, M. Zhu, Q. Shi, F. Wen, L. Liu, B. Dong, A. Haroun, Y. Yang, P. Vachon, X. Guo, T. He, C. Lee, Progress inTENGtechnology—A journey from energy harvesting to nanoenergy and nanosystem, EcoMat 2 (4) (2020), e12058.
[62] H. Wang, J. Zhu, T. He, Z. Zhang, C. Lee, Programmed-triboelectric nanogenerators—a multi-switch regulation methodology for energy manipulation, Nano Energy 78 (2020), 105241.
[63] J. Zhu, H. Wang, Z. Zhang, Z. Ren, Q. Shi, W. Liu, C. Lee, Continuous direct current by charge transportation for next-generation IoT and real-time virtual reality applications, Nano Energy 73 (2020), 104760.
[64] J. Zhu, X. Liu, Q. Shi, T. He, Z. Sun, X. Guo, W. Liu, O. Sulaiman, B. Dong, C. Lee, Development trends and perspectives of future sensors and MEMS/NEMS, Micromachines 11 (7) (2020) 541.
[65] Y. Liu, J. Mo, Q. Fu, Y. Lu, N. Zhang, S. Wang, S. Nie, Enhancement of triboelectric charge density by chemical functionalization, Adv. Funct. Mater. 30 (50) (2020), 2004714.

[66] S. Nie, H. Guo, Y. Lu, J. Zhuo, J. Mo, Z. Wang, Superhydrophobic cellulose paper-based triboelectric nanogenerator for water drop energy harvesting, Adv. Mater. Technol. 5 (9) (2020), 2000454.
[67] C. Cai, J. Mo, Y. Lu, N. Zhang, Z. Wu, S. Wang, S. Nie, Integration of a porous wood-based triboelectric nanogenerator and gas sensor for real-time wireless food-quality assessment, Nano Energy 83 (2021), 105833.
[68] T. He, H. Wang, J. Wang, X. Tian, F. Wen, Q. Shi, J. Ho, C. Lee, Self-sustainable wearable textile nano-energy nano-system (NENS) for next-generation healthcare applications, Adv. Sci. 6 (2019), 1901437.
[69] B. Lebental, W. Moujahid, C. Lee, J. Maurice, C. Cojocaru, Graphene-based resistive humidity sensor for in-situ monitoring of drying shrinkage and intrinsic permeability in concrete. 4th International Symposium on Nanotechnology in Construction. 2012 May, 1–8.
[70] A. Smith, K. Elgammal, F. Niklaus, A. Delin, A. Fischer, S. Vaziri, F. Forsberg, M. Råsander, H. Hugosson, L. Bergqvist, S. Schröder, S. Kataria, M. Östlinga, M. Lemme, Resistive graphene humidity sensors with rapid and direct electrical readout, Nanoscale 7 (2015) 19099–19109.
[71] E. Alenezy, Y. Sabri, A. Kandjani, D. Korcoban, S. Rashid, S. Ippolito, S. Bhargava, Low-temperature hydrogen sensor: enhanced performance enabled through photoactive Pd-decorated TiO_2 colloidal crystals, ACS Sens. 5 (12) (2020) 3902–3914.